Inventum Biologicum: *An International Journal of Biological Research*
2026, Vol. 6, Issue 3, pp. 56-64

Inventum Biologicum

Journal homepage: www.journals.worldbiologica.com/ib

Research paper

Green Synthesis of Carbon Quantum Dots from *Cadaba fruticosa* Flower for Photocatalytic Degradation of Methylene Blue, Rose Bengal, and Bromophenol Blue Dyes

B. Mallikarjuna [a]*, **S. K. Esub Basha** [b], **Shadik Ahmed Mohammed** [c], **Merugu Santha Kumari** [d], **K. G. Venkatesh** [a], **Abhinash Marukurti** [e]

[a] *Department of Chemistry, SRR & CVR Government Degree College (A) Vijayawada, Andhra Pradesh, India*
[b] *Department of Physics, SRR & CVR Government Degree College (A) Vijayawada, Andhra Pradesh, India*
[c] *Department of Chemistry, Government Degree College, Kovvur, Andhra Pradesh, India*
[d] *Department of Chemistry, DRG Government Degree College, Tadepalligudem, Andhra Pradesh, India*
[e] *School of Life and Health Sciences, Adikavi Nannaya University, Rajamahendravaram, Andhra Pradesh, India*

ARTICLE INFO

Keywords

Carbon quantum dots
Cadaba fruticosa
Rose Bengal
bromophenol blue
wastewater treatment

DOI
10.5281/ib-2572026

***Corresponding author**
B. Mallikarjuna

Email
drmallichem@srrcvr.ac.in

ABSTRACT

Synthetic dyes discharged from textile, printing, and cosmetic industries are a major source of aquatic pollution, and there is a pressing need for low-cost, eco-friendly remediation photocatalysts. In this study, fluorescent carbon quantum dots (CQDs) were green-synthesized from *Cadaba fruticosa* flowers by a rapid, single-step microwave-assisted route and evaluated as visible-light photocatalysts for the degradation of three structurally distinct dyes: methylene blue (MB, cationic thiazine), Rose Bengal (RB, anionic xanthene), and bromophenol blue (BPB, halogenated sulfonphthalein). The CQDs were characterized by UV-Visible absorption spectroscopy (absorption maxima at 239 and 277 nm, assigned to π–π* and n–π* transitions), Fourier-transform infrared (FTIR) spectroscopy (C–H, C≡C, C=N and C–Br surface functionalities), powder X-ray diffraction (broad amorphous carbon halo with an average crystallite size of 21.26 ± 8.91 nm by the Debye–Scherrer equation), dynamic light scattering (DLS; principal population 1–10 nm, PDI 0.474), zeta potential (−3.56 mV), and fluorescence spectroscopy (stable emission at 538, 576 and 621 nm). Under visible-light irradiation, the CQDs degraded MB most effectively, reaching 85% and 66% removal at 50 and 100 µg/mL CQD loading, respectively, within 90 minutes, while RB (16–20%) and BPB (9–11%) were degraded to a much lower extent, reflecting the influence of dye charge, structure, and halogenation on adsorption and reactive-oxygen-species-mediated breakdown. These results establish *Cadaba fruticosa* flower-derived CQDs as a sustainable, low-cost nanomaterial with selective photocatalytic activity toward cationic dye pollutants and provide a mechanistic basis for further optimization toward broader-spectrum dye remediation.

1. Introduction

Dyes are coloured aromatic organic compounds used to impart permanent colour to substrates in the textile, food, rubber, printing, cosmetic, medicinal, and paper industries. Over 100,000 commercial dyes are in use worldwide, and it is estimated that roughly 12% of the dye consumed during processing is lost as effluent, with about 20% of that loss entering natural water bodies [1,2]. Because most synthetic dyes are chemically stable, resistant to biodegradation, and often carcinogenic or mutagenic, their accumulation in aquatic systems poses serious ecological and public-health risks, compounded by the fact that more than a billion people already lack access to adequate

clean water [3]. Methylene blue (MB), a cationic thiazine dye first synthesized in the nineteenth century, is one of the most heavily used textile colourants; chronic exposure has been linked to skin irritation, nervous system disturbances and cardiovascular effects [4,5]. Rose Bengal (RB), an anionic xanthene dye used extensively in printing and biological staining, is cytotoxic to human cells, producing membrane disruption, vacuolation and lysis [6]. Bromophenol blue (BPB), a halogenated sulfonphthalein indicator dye, is listed by the United States Environmental Protection Agency among priority toxic halogenated phenols owing to its genotoxic, mutagenic and carcinogenic potential and its resistance to natural degradation [7]. Conventional treatment strategies for dye-laden effluent such as adsorption, ion exchange, biodegradation, and advanced oxidation andeach carry limitations of cost, secondary waste generation, or incomplete mineralization, motivating continued interest in semiconductor- and carbon-based photocatalysts that can be produced sustainably [6,8].

Carbon dots (CDs), and their crystalline sub-class carbon quantum dots (CQDs), are quasi-spherical carbon nanostructures typically below 10 nm in diameter that combine tunable photoluminescence, excellent aqueous dispersibility, low toxicity, and facile, low-cost synthesis [9,10]. Two broad synthetic philosophies are recognized: "top-down" approaches that fragment bulk carbon precursors (arc discharge, laser ablation, chemical/electrochemical oxidation) into nanoscale particles, and "bottom-up" approaches that build CDs from small molecular or biomass precursors through hydrothermal/solvothermal treatment, pyrolysis, or microwave-assisted carbonization [9,11]. Among these, microwave-assisted synthesis has gained particular traction because it is rapid, scalable, energy-efficient, and solvent-minimal: microwave irradiation couples directly with polar precursor molecules, producing fast, homogeneous in-situ heating that improves both the yield and the optical quality of the resulting CDs relative to conventional heating [11,12].

Plant biomass has emerged as an especially attractive CD precursor because it is renewable, inexpensive, and naturally rich in the carbohydrates, polyphenols and amino compounds that carbonize into fluorescent nanostructures while simultaneously furnishing surface hydroxyl, carboxyl and amine groups that enhance water dispersibility and reactivity [10,13]. Reported plant-derived CDs include those obtained from date kernels, groundnut shells, pineapple peel, rose flowers, olive solid waste, chicken feathers, coconut husk, rubber-seed shells, sugarcane bagasse, garden thyme, sorghum, and crab shell/other biomass wastes, several of which have shown promising activity toward the photocatalytic decolourization of methylene blue, Rose Bengal, methyl orange, and related pollutants [14–22]. *Cadaba fruticosa* flower, a shrub traditionally used in folk medicine across the Indian subcontinent, is valued for its phytochemical-rich leaves and flowers and has recently attracted nanotechnological interest: aqueous extracts of its leaves have been used to green-synthesize silver and cupric oxide nanostructures with demonstrated antibacterial, antioxidant and photocatalytic properties [24–26]. However, to the best of our knowledge, no previous study has synthesized CQDs from *Cadaba fruticosa* flower by a microwave-assisted green route and systematically evaluated their photocatalytic activity toward multiple structurally distinct dye classes in parallel.

In the present work, we report a simple, one-step microwave-assisted synthesis of fluorescent CQDs from *Cadaba fruticosa* flowers and their comprehensive physicochemical characterization by UV-Visible absorption spectroscopy, FTIR spectroscopy, powder XRD, dynamic light scattering, zeta potentiometry, and fluorescence spectroscopy. We then benchmark the visible-light photocatalytic performance of these CQDs, at two catalyst loadings (50 and 100 µg/mL), against three dyes of contrasting charge and structure, the cationic dye methylene blue, the anionic xanthene dye Rose Bengal, and the halogenated indicator dye bromophenol blue to establish structure–activity trends that can guide the future design of plant-derived carbon nanomaterial photocatalysts for wastewater remediation.

2. Materials and Methods

2.1 Chemicals and instrumentation

Methylene blue (Hi-Media), Rose Bengal (Hi-Media) and bromophenol blue (CDH) were used as received, along with double-distilled water. Instrumentation comprised a magnetic stirrer (Remi), an analytical weighing balance (Shimadzu), a refrigerated centrifuge (Eppendorf), a UV-Visible spectrophotometer, a Fourier-transform infrared spectrometer, a fluorescence spectrophotometer with a UV-transilluminator (254/312 nm), a powder X-ray diffractometer (Bruker, Cu-Kα1 radiation, λ = 0.15406 nm), a particle-size/zeta-potential analyser (Malvern), a household microwave oven (LG), and a distilled-water purification unit (Borosil). Standard laboratory glassware, muslin cloth, Whatman No.1 filter paper, PVDF syringe filters (0.22 µm), quartz/glass cuvettes and 2 mL Eppendorf tubes were used throughout.

2.2 Collection and processing of plant material

The flowers of *Cadaba fruticosa* collected and were rinsed under running tap water followed by double-distilled water, shade-dried, and ground to a fine powder using an electric blender prior to synthesis.

2.3 Microwave-assisted green synthesis of CQDs

Two grams of dried flower powder were dispersed in 100 mL of distilled water and stirred at 100 °C on a magnetic stirrer. The homogenized suspension was then irradiated in a domestic microwave oven at 900 W in repeated 10-second pulses separated by 30-second cooling intervals, for a total irradiation time of 6 minutes. After the reaction mixture cooled to room temperature, it was filtered through muslin cloth to remove coarse debris, and the filtrate was centrifuged at 10,000 rpm for 10 minutes; the supernatant was retained and the pellet discarded. The supernatant was sequentially filtered through Whatman No.1 filter paper and a 0.22 µm PVDF syringe filter to yield an optically clear, aqueous CQD stock solution, which was stored at 4 °C in the dark until use.

2.4 Physicochemical characterization

UV-Visible spectroscopy: CQDs were diluted 9:1 with distilled water and scanned from 200–800 nm on the UV-2600 spectrophotometer to evaluate surface plasmon/electronic transitions; raw spectra were processed in OriginPro.

FTIR spectroscopy: 100 µL of CQD solution was cast onto a KBr pellet and scanned from 500–4000 cm^{-1} to identify surface functional groups, referenced against standard IR correlation tables.

X-ray diffraction: CQDs were solidified at 70 °C and ground to a fine powder for XRD analysis using monochromatic Cu-Kα1 radiation. Crystallite size (D) was calculated from the Debye–Scherrer equation, $D = K\lambda/(\beta \cos \theta)$, where K is the shape factor (0.94), λ is the X-ray wavelength (0.15406 nm), β is the full width at half-maximum (FWHM, radians) and θ is the Bragg angle (radians).

Dynamic light scattering and zeta potential: Hydrodynamic size distribution (0.1–10,000 nm) and surface charge were measured on the Malvern particle-size/zeta-potential analyser across a temperature range of 20–120 °C.

Fluorescence spectroscopy: Excitation/emission scans (200–900 nm, zero-order selectable) were recorded on the PerkinElmer fluorescence spectrophotometer, and qualitative emission was additionally visualized under 254 nm and 312 nm UV-transillumination.

2.5 Photocatalytic dye-degradation assay

MB, RB and BPB stock dyes were each prepared at 10 ppm (10 µg/mL) in distilled water. Two CQD working concentrations were prepared: 50 µg/mL (S1) and 100 µg/mL (S2). For each trial, CQDs (S1 or S2) were added to 50 mL of dye solution in a conical flask and pre-incubated in a dark chamber with stirring for 30 minutes to establish adsorption–desorption equilibrium. The flasks were then exposed to visible light from a 100 W lamp positioned 10 cm from the flask. At 15-minute intervals over 90 minutes (time points T1–T6), a 4 mL aliquot was withdrawn, centrifuged at 10,000 rpm for 5 minutes at 4 °C, and the supernatant analysed by UV-Visible spectrophotometry: 450–650 nm for MB (λmax 664 nm, control OD 1.814), 400–650 nm for RB (λmax 550 nm, control OD 0.811), and 480–660 nm for BPB (λmax 590 nm, control OD 1.394). Percentage degradation was calculated as:

$$\% \text{ Degradation} = [(\text{Control OD} - \text{Sample OD}) / \text{Control OD}] \times 100$$

3. Results and Discussion

3.1 UV-Visible absorption spectroscopy

The aqueous CQD solution displayed two characteristic absorption features at 239 nm and 277 nm (Figure 1A), consistent with π–π* transitions of aromatic C=C domains in the carbogenic core and n–π* transitions of surface C=O groups, respectively [10]. This two-peak absorption profile in the 230–330 nm region is a widely reported optical signature of plant-derived CDs: CDs isolated hydrothermally from rose flowers absorb at 270 and 360 nm [10], while CDs from date kernel, groundnut and pineapple peel show comparable π–π* absorption between 275–280 nm [11], and CQDs derived from chicken feathers absorb at 215 and 275 nm [18]. The close agreement between the present *Cadaba fruticosa* flower CQDs and these independently reported biomass-derived carbon dots supports successful CQD formation via the microwave-assisted route.

3.2 FTIR spectroscopy

FTIR analysis (Figure 1B) resolved four principal absorption features: a strong, sharp band at 3329.66 cm⁻1 assigned to C–H stretching, a weak band at 2105.76 cm⁻1 consistent with C≡C stretching of alkyne-type residues, a medium band at 1638.05 cm⁻1 attributed to C=N stretching (imine/oxime character), and a strong broad band at 521.29 cm⁻1 associated with C–Br stretching, indicative of halogenated surface residues inherited from the plant matrix (Table 1). Similar oxygen/nitrogen-rich functionalization has been reported for CDs derived from crab shell (O–H/N–H/C=O/C=C features at 3398, 2930, 1640, 1563 and 1415 cm⁻1) [10] and pipe tobacco (O–H, carboxylic and alkyl features at 3427, 1701, 1517, 1282, 1117, 2968 and 2935 cm⁻1) [9], confirming that the microwave-assisted carbonization of *Cadaba fruticosa* flower retains abundant polar surface chemistry an important prerequisite for the aqueous dispersibility and photocatalytic reactivity of the CQDs.

Table 1 FTIR absorbance peaks and corresponding functional groups of *Cadaba fruticosa* flower-derived CQDs

Peak (cm^{-1})	Appearance	Functional group	Assigned compound class
521.29	Strong	C–Br stretching	Halo compound
1638.05	Medium	C=N stretching	Imine / oxime
2105.76	Weak	C≡C stretching	Alkyne
3329.66	Strong, sharp	C–H stretching	Alkyne / terminal C–H

3.3 X-ray diffraction

The powder XRD pattern (Figure 1C) shows a broad diffuse hump centred near 2θ ≈ 20–25°, characteristic of amorphous/turbostratic carbon, superimposed with seventeen discernible diffraction peaks at 2θ = 3.84°, 5.05°, 28.52°, 31.85°, 35.88°, 40.71°, 45.57°, 50.37°, 56.73°, 58.94°, 66.66°, 73.99°, 75.38°, 87.83°, 94.75°, 101.73° and 108.77° (Table 2). Applying the Debye–Scherrer equation to each reflection gave individual crystallite sizes ranging from ≈ 4 to 38 nm, with an average crystallite size of 21.26 ± 8.91 nm across all seventeen peaks closely matching the 21.2636 nm value obtained by averaging the full peak set. The broad low-angle hump combined with sharp superimposed reflections is consistent with a graphitic-core/amorphous-shell nanostructure typical of biomass-derived CDs; a comparable broad peak near 2θ = 28.5° (graphitic (002) plane) with a weaker reflection near 40.3° has been reported for hydrothermally synthesized kiwi-fruit-derived CDs [9].

Table 2 Representative XRD diffraction peaks (2θ) and Debye–Scherrer crystallite sizes of CQDs (selected peaks; full 17-peak dataset used for the average)

Peak label	2θ (degree)	Crystallite size, D (nm)
P1	3.84	113.73
P3	28.52	380.89
P6	40.71	330.22
P9	56.73	245.87
P11	66.66	254.57
P14	87.83	112.23
P17	108.77	228.28
Average (all 17 peaks)	—	**21.26 ± 8.91**

3.4 Dynamic light scattering and zeta potential

DLS analysis of the CQD suspension (Figure 1D) revealed a bimodal intensity-weighted size distribution: a primary population centred between 1–10 nm with a polydispersity index (PDI) of 0.474, consistent with the nanoscale carbon core detected by XRD, and a secondary population near 700–1000 nm that most likely reflects loose CQD aggregation or minor particulate contamination arising from prolonged sample handling rather than the intrinsic CQD size. Zeta-potential measurement (Figure 1E) gave a value of −3.56 mV, indicating a weakly anionic surface consistent with the carboxyl/hydroxyl functionalities detected by FTIR. Although zeta potentials more negative than −30 mV are generally required for strong electrostatic (charge-repulsion) colloidal stability, and values between −10 and +10 mV are classified as effectively neutral [12], the moderate negative surface charge of the present CQDs is broadly consistent with other biomass-derived CDs for example, coriander-leaf-derived CDs synthesized hydrothermally showed a more strongly negative zeta potential of −24.9 mV, attributed to abundant surface hydroxyl and carboxylic groups [9]. The comparatively weaker surface charge of the *Cadaba fruticosa* flower CQDs suggests that colloidal stability in this system is likely supplemented by steric stabilization from surface-bound phytochemical residues rather than electrostatic repulsion alone.

3.5 Fluorescence spectroscopy

Under UV-transillumination at 254 nm and 312 nm the CQD solution exhibited visible blue-region fluorescence (Figure 1F), with quantitative emission scans showing stable, well-resolved peaks at 538 nm, 576 nm and 621 nm. The dependence of emission wavelength on excitation wavelength is a hallmark optical property of CDs and has been attributed variously to differences in surface energy-trap states, particle-size distribution, and degree of π-conjugation within the carbogenic core [19]. Excitation-dependent, size-tunable photoluminescence spanning the visible-to-near-infrared region has been demonstrated computationally and experimentally for graphene quantum dots of varying diameter (0.46–2.31 nm), where the smallest particles emit near 235 nm and the largest near 999.5 nm [15]; the stable multi-peak visible emission observed here is consistent with a heterogeneous, moderately polydisperse CQD population, in agreement with the DLS results.

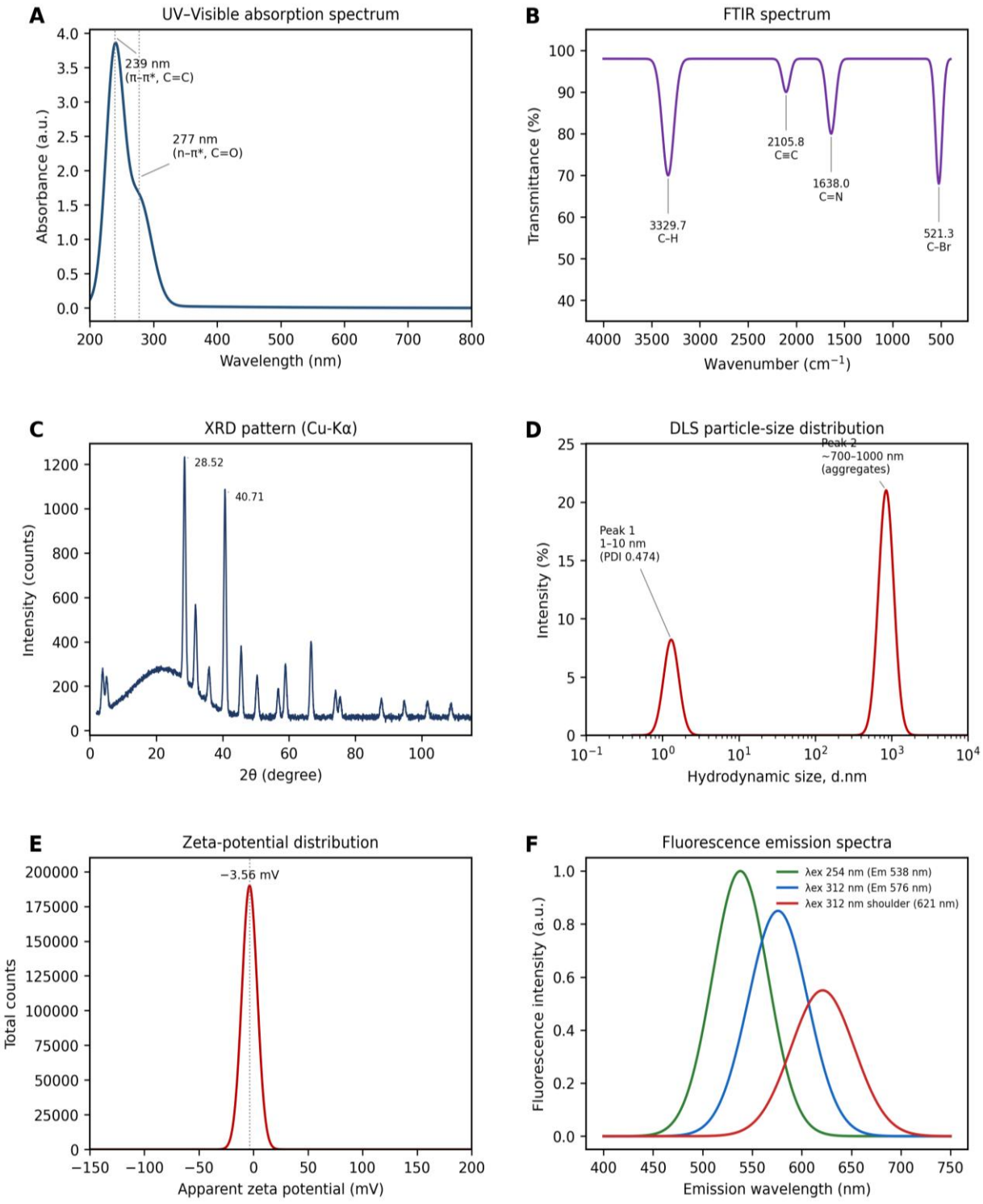

Fig. 1 Physicochemical characterization of *Cadaba fruticosa* flower-derived CQDs. (A) UV-Visible absorption spectrum showing π–π* (239 nm) and n–π* (277 nm) transitions. (B) FTIR transmittance spectrum with assigned functional groups. (C) Powder XRD pattern (Cu-Kα) showing the amorphous carbon halo and superimposed crystalline reflections. (D) DLS particle-size distribution by intensity. (E) Zeta-potential distribution. (F) Fluorescence emission spectra at 254 nm and 312 nm excitation

3.6 Photocatalytic degradation of dyes

Photocatalytic degradation of synthetic dyes has been an actively pursued remediation strategy since the latter half of the twentieth century, gaining renewed urgency as textile, leather, furniture and plastics industries continue to discharge large volumes of dye-contaminated wastewater [2,23]. The photocatalytic performance of the *Cadaba fruticosa* flower CQDs was evaluated in parallel against three dyes of contrasting molecular charge and structure — the cationic dye MB, the anionic dye RB, and the halogenated dye BPB — at two catalyst loadings (50 and 100 µg/mL) under visible-light irradiation for 90 minutes.

3.6.1 Methylene blue

Time-resolved absorption spectra of MB in the presence of CQDs (Figure 2A, B) show a progressive decrease in the characteristic 664 nm absorption band across the T1–T6 sampling points at both catalyst loadings. Maximum degradation reached 85% at 50 µg/mL CQDs and 66% at 100 µg/mL CQDs after 90 minutes (Figure 2C), with the lower catalyst loading unexpectedly outperforming the higher loading — a trend that may reflect self-shielding/light-scattering effects at higher CQD concentrations, which can reduce photon penetration and the availability of activated surface sites, an effect previously noted for other nanoparticle photocatalysts operating above their optimal dosage [3]. The present degradation efficiency is broadly comparable to, though somewhat lower than, several other biomass-derived carbon nanomaterial systems: N-doped ZnO/carbon-dot nanocomposites synthesized from organic soybean achieved 83.4% MB decolorization under UV-B irradiation, considerably outperforming ZnO alone (70.3%) and CDs alone (9.48%) [22], while tungsten-oxide/amino-CQD composites derived from sugarcane bagasse improved MB degradation from 84.6% (CQDs alone) to 92.9% upon compositing [21], and CuO nanoparticles green-synthesized from *Cadaba fruticosa* flower extract have independently been shown to be effective MB photocatalysts under visible light [24]. These comparisons suggest that compositing the present CQDs with a wide-bandgap semiconductor (e.g., ZnO or TiO_2) could substantially enhance MB removal beyond the single-component CQD system reported here.

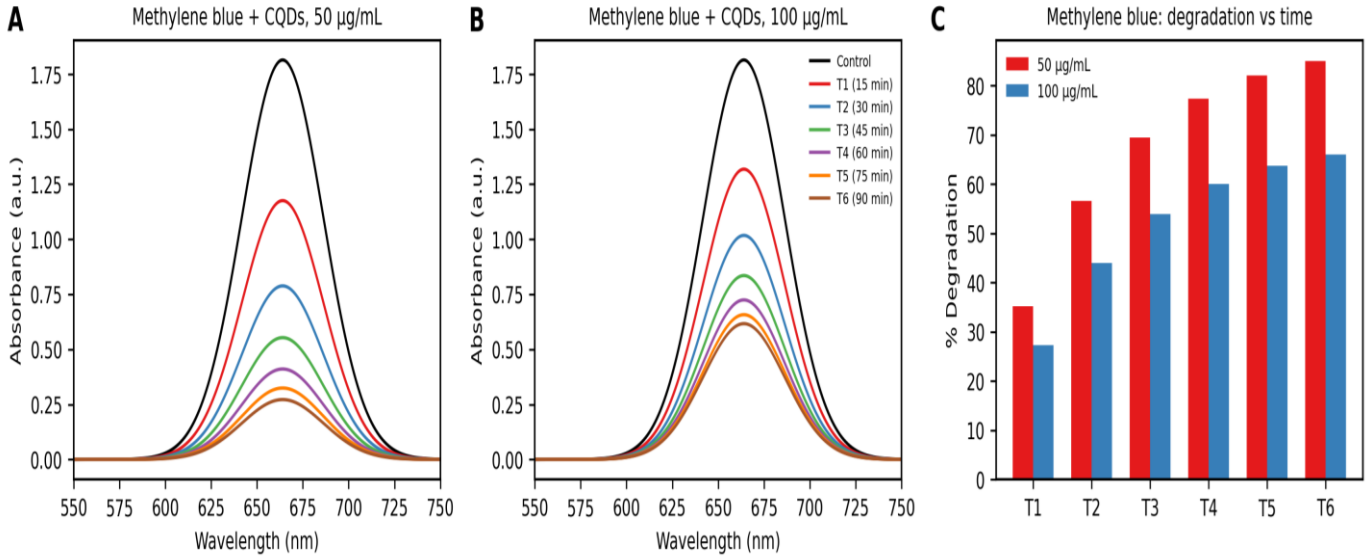

Fig. 2 Photocatalytic degradation of methylene blue (MB) by *Cadaba fruticosa* flower CQDs. (A) Time-resolved UV-Vis absorption spectra at 50 µg/mL CQDs. (B) Time-resolved UV-Vis absorption spectra at 100 µg/mL CQDs. (C) Percentage degradation at each 15-minute interval (T1–T6) for both concentrations

3.6.2 Rose Bengal

RB degradation was markedly lower than MB, reaching only 16% at 50 µg/mL and 20% at 100 µg/mL CQDs after 90 minutes (Figure 3A–C), with the higher catalyst dose here providing a modest improvement, in contrast to the trend observed for MB. RB is an anionic dye at neutral pH; electrostatic repulsion between the weakly negative CQD surface (zeta potential −3.56 mV) and the anionic dye likely limits adsorption-driven contact and, in turn, the efficiency of reactive-oxygen-species-mediated oxidation. This is consistent with the substantially higher RB removal efficiencies reported for photocatalysts bearing a more strongly positive or neutral surface character: metal-free triazine-based covalent organic polymer/porous g-C3N4 composites achieved 82.3% RB degradation [8], sorghum-derived carbon dots produced by pyrolysis have been systematically optimized for RB removal [17], and garlic-derived carbon dots (fabricated at 300 °C) improved RB decontamination from 74.5% to 91.1% with increasing pyrolysis time [6]. Taken together, these results indicate that surface-charge engineering — for example, cationic surface functionalization of the present CQDs — represents a promising strategy to improve their activity toward anionic dyes such as RB.

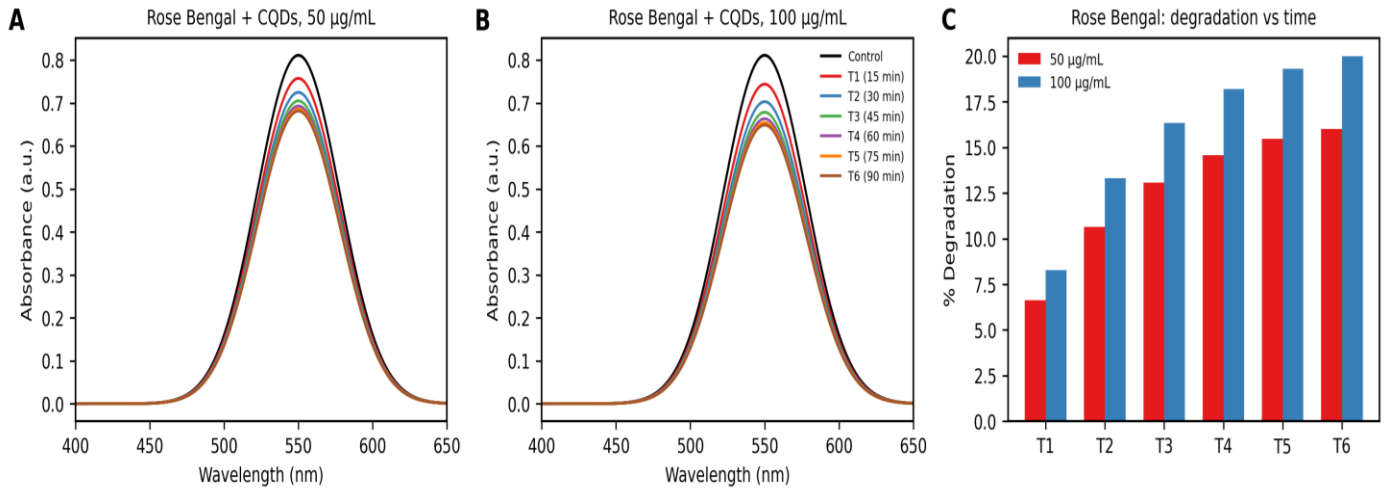

Fig. 3 Photocatalytic degradation of Rose Bengal (RB) by *Cadaba fruticosa* flower CQDs. (A) Time-resolved UV-Vis absorption spectra at 50 µg/mL CQDs. (B) Time-resolved UV-Vis absorption spectra at 100 µg/mL CQDs. (C) Percentage degradation at each 15-minute interval (T1–T6) for both concentrations

3.6.3 Bromophenol blue

BPB proved the most recalcitrant of the three dyes, with maximum degradation of only 11% at 50 µg/mL and 9% at 100 µg/mL CQDs (Figure 4A–C). This low removal efficiency is consistent with the chemical robustness conferred by BPB's brominated sulfonphthalein structure, which is inherently resistant to oxidative attack — the same property responsible for its listing as a persistent, slow-degrading halogenated pollutant [7]. Comparable difficulty in BPB photodegradation has been documented for other nanomaterial photocatalysts: TiO2 nanoparticles required a very high loading of 1 g/L to remove 85% of BPB [28], while sol-gel-synthesized TiO2 achieved only 13.5% BPB removal at low loading, rising to 88.5% only after compositing with poly(3-hexylthiophene) (TiO2/P3HT) and prolonged (10 h) UV irradiation [28]. The present single-component CQD system, evaluated here under considerably milder visible-light conditions and shorter irradiation time (90 min), therefore performs within the expected range for an unmodified, non-composited carbon photocatalyst, and indicates that C–Br bond cleavage — rather than simple dye-chromophore oxidation — is likely rate-limiting for BPB removal.

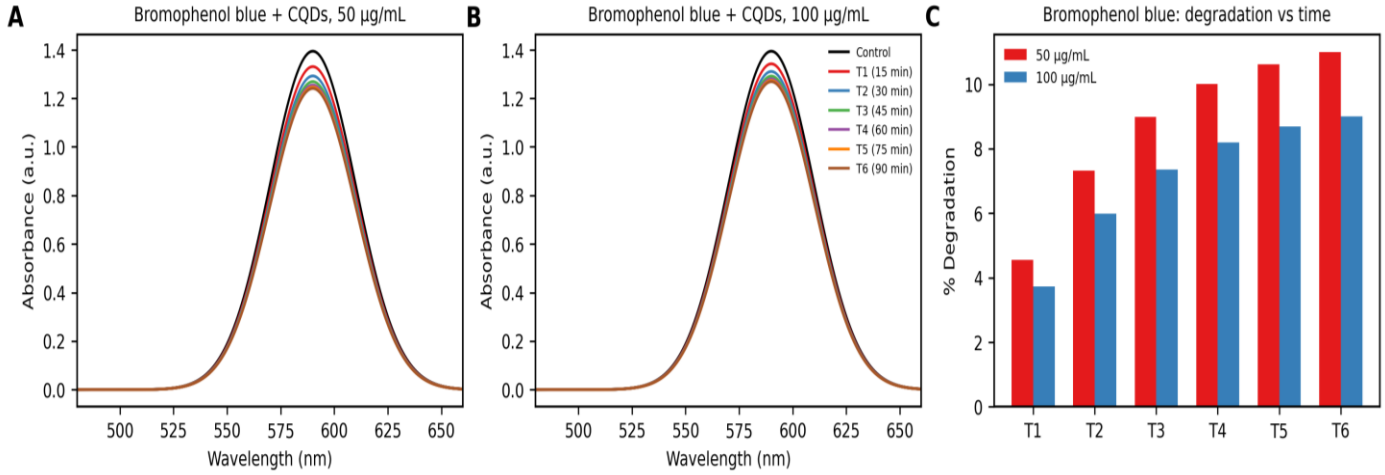

Fig. 4 Photocatalytic degradation of bromophenol blue (BPB) by *Cadaba fruticosa* flower CQDs. (A) Time-resolved UV-Vis absorption spectra at 50 µg/mL CQDs. (B) Time-resolved UV-Vis absorption spectra at 100 µg/mL CQDs. (C) Percentage degradation at each 15-minute interval (T1–T6) for both concentrations

3.6.4 Comparative degradation performance

Figure 5 summarizes the maximum degradation achieved for all three dyes at both CQD loadings. The clear rank order — MB (66–85%) ≫ RB (16–20%) > BPB (9–11%) — highlights that dye charge and chemical structure, rather than catalyst loading alone, are the dominant determinants of photocatalytic removal efficiency in this system. The pronounced selectivity toward the cationic dye MB is consistent with favourable electrostatic and π-stacking interactions between MB and the CQD surface, while the anionic (RB) and halogenated (BPB) dyes are comparatively disfavoured. These structure–activity trends provide a practical basis for targeting the

present *Cadaba fruticosa* flower CQDs toward cationic-dye-dominated effluent streams, and motivate future work on surface functionalization or semiconductor compositing to broaden their activity spectrum.

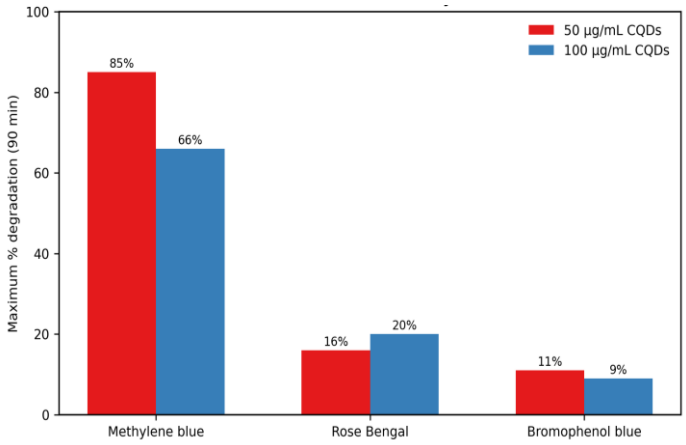

Fig. 5 Comparative maximum photocatalytic degradation (90 min) of methylene blue, Rose Bengal and bromophenol blue by *Cadaba fruticosa* flower CQDs at 50 and 100 µg/mL loading

4. Conclusion

Fluorescent carbon quantum dots were successfully synthesized from *Cadaba fruticosa* flowers using a rapid, single-step, microwave-assisted green route. Comprehensive characterization confirmed the formation of small (1–10 nm core), oxygen/nitrogen-functionalized, weakly anionic, fluorescent CQDs with an amorphous-carbon XRD signature and an average crystallite size of 21.26 nm. Under visible-light irradiation, the CQDs displayed selective photocatalytic activity, degrading the cationic dye methylene blue substantially more effectively (66–85%) than the anionic dye Rose Bengal (16–20%) or the halogenated dye bromophenol blue (9–11%), pointing to electrostatic dye–catalyst interaction and chemical recalcitrance (halogenation) as key determinants of degradation efficiency. These findings establish *Cadaba fruticosa* flower waste as a viable, low-cost, renewable precursor for fluorescent carbon nanomaterials with practical potential in the visible-light photocatalytic remediation of cationic-dye-contaminated wastewater, and identify semiconductor compositing and surface-charge engineering as promising directions for extending this activity to anionic and halogenated dye classes.

Conflict of Interest

The authors declare no conflict of interest.

References

1. I. Khan et al., "Review on Methylene Blue: Its Properties, Uses, Toxicity and Photodegradation," Water (Switzerland), vol. 14, no. 2, 2022, doi: 10.3390/w14020242.
2. B. Viswanathan, "Photocatalytic Degradation of Dyes: An Overview," Curr. Catal., vol. 7, no. 2, pp. 99–121, 2017, doi: 10.2174/2211544707666171219161846.
3. A. Ajmal, I. Majeed, R. N. Malik, H. Idriss, and M. A. Nadeem, "Principles and mechanisms of photocatalytic dye degradation on TiO2 based photocatalysts: A comparative overview," RSC Adv., vol. 4, no. 70, pp. 37003–37026, 2014, doi: 10.1039/c4ra06658h.
4. H. Xue, A. Thaivalappil, and K. Cao, "The potentials of methylene blue as an anti-aging drug," Cells, vol. 10, no. 12, pp. 1–10, 2021, doi: 10.3390/cells10123379.
5. D. G. Ayu et al., "Photocatalytic Degradation of Methylene Blue Using N-Doped ZnO/Carbon Dot (N-ZnO/CD) Nanocomposites Derived from Organic Soybean," ACS Omega, vol. 8, no. 17, pp. 14965–14984, 2023, doi: 10.1021/acsomega.2c07546.
6. S. Kumar, "Preprint: garlic-derived carbon dots for decontamination of Rose Bengal dye by pyrolysis approach," (preprint, not peer reviewed).
7. R. Shanker Sahu, A. Dubey, and Y. hsin Shih, "Novel metal-free in-plane functionalized graphitic carbon nitride with graphene quantum dots for effective photodegradation of 4-bromophenol," Carbon N. Y., vol. 182, pp. 89–99, 2021, doi: 10.1016/j.carbon.2021.05.033.
8. S. Anwer, A. Bharath, R. Gopinath, K. Krishnan, and P. Balakrishnan, "A Novel Nanocomposite Based on Triazine Based Covalent Organic Polymer Blended with Porous g-C3N4 for Photo Catalytic Dye Degradation of Rose Bengal and Fast Green," PMC, 2022.
9. K. J. Mintz et al., "A deep investigation into the structure of carbon dots," Carbon N. Y., vol. 173, pp. 433–447, 2021, doi: 10.1016/j.carbon.2020.11.017.
10. H. H. Jing et al., "Green Carbon Dots: Synthesis, Characterization, Properties and Biomedical Applications," J. Funct. Biomater., vol. 14, no. 1, 2023, doi: 10.3390/jfb14010027.
11. M. Zulfajri, H. N. Abdelhamid, S. Sudewi, and S. Dayalan, "Plant Part-Derived Carbon Dots for Biosensing."
12. B. D. Mansuriya and Z. Altintas, "Carbon dots: Classification, properties, synthesis, characterization, and applications in health care — an updated review (2018–2021)," Nanomaterials, vol. 11, no. 10, 2021, doi: 10.3390/nano11102525.
13. P. Kumar, S. Dua, R. Kaur, M. Kumar, and G. Bhatt, "A review on advancements in carbon quantum dots and their application in photovoltaics," RSC Adv., vol. 12, no. 8, pp. 4714–4759, 2022, doi: 10.1039/d1ra08452f.
14. L. Cui, X. Ren, M. Sun, H. Liu, and L. Xia, "Carbon dots: Synthesis, properties and applications," Nanomaterials, vol. 11, no. 12, 2021, doi: 10.3390/nano11123419.
15. M. Imran Din et al., "Novel and Facile Synthesis of Carbon Quantum Dots from Chicken Feathers and Their Application as a Photocatalyst to Degrade Methylene Blue Dye," J. Chem., vol. 2023, 2023, doi: 10.1155/2023/9956427.
16. Sk, M. P. et al., "Quantum confinement effect and photoluminescence of zigzag-edged graphene quantum dots," as cited in reviews of GQD photoluminescence tunability.
17. S. Sawalha, H. Azzam, R. Bin Ali, H. Dweikat, and K. Anaya, "Photodegradation of Methylene Blue by Carbon Nanodots Synthesized from Olive Solid Wastes," pp. 12–14, 2021.

18. S. T, A. T., G. A, and K. J, "Phytochemical, FTIR and GCMS Analysis and Antibacterial Activity of Methanol Extract of Leaf and Flower of *Cadaba fruticosa* flower," Int. J. Zool. Investig., vol. 7, no. 2, pp. 997–1008, 2021, doi: 10.33745/ijzi.2021.v07i02.091.
19. P. K. B, R. Kant, R. Lall, A. Verma, and P. Verma, Proceedings of BioSangam 2022: Emerging Trends in Biotechnology, vol. 1. Atlantis Press International BV, 2023, doi: 10.2991/978-94-6463-020-6.
20. M. Jorns and D. Pappas, "A Review of Fluorescent Carbon Dots, Their Synthesis, Physical and Chemical Characteristics, and Applications," 2021.
21. D. Stefanakis, A. Philippidis, L. Sygellou, G. Filippidis, D. Ghanotakis, and D. Anglos, "Synthesis of fluorescent carbon dots by a microwave heating process: structural characterization and cell imaging applications," J. Nanoparticle Res., vol. 16, no. 10, 2014, doi: 10.1007/s11051-014-2646-1.
22. N. Kendre and P. Wakte, "A review on Phytochemicals and biological attributes of *Cadaba fruticosa* flower," Asian J. Pharm. Pharmacol., vol. 7, no. 2, pp. 74–84, 2021, doi: 10.31024/ajpp.2021.7.2.2.
23. K. J. Konstantinou and T. A. Albanis, cited in reviews of industrial dye stuffs as toxic organic pollutants.
24. P. Das, S. Ghosh, R. Ghosh, S. Dam, and M. Baskey, "*Cadaba fruticosa* flower plant mediated green synthesis of cupric oxide nanoparticles: A promising environmentally sustainable material for waste water treatment and efficient antibacterial agent," J. Photochem. Photobiol. B Biol., vol. 189, pp. 66–73, 2018, doi: 10.1016/j.jphotobiol.2018.09.023.
25. A. Kamal, "Qualitative Phytochemical Analysis of *Cadaba fruticosa* flower," Int. J. Plant Sci., vol. 3, no. 4, pp. 38–41, 2014.
26. D. N and S. R, "*Cadaba fruticosa* flower (Sapotaceae): A Review of its Phytochemical and Pharmacological Profile," Int. J. Pharma Bio Sci., vol. 7, no. 4, 2016, doi: 10.22376/ijpbs.2016.7.4.b106-114.
27. Y. Liu, Y. Huang, A. Xiao, H. Qiu, and L. Liu, "Preparation of magnetic Fe3O4/MIL-88A nanocomposite and its adsorption properties for bromophenol blue dye in aqueous solution," Nanomaterials, vol. 9, no. 1, 2019, doi: 10.3390/nano9010051.
28. J. Dhanalakshmi and D. P. Padiyan, "Photocatalytic degradation of methyl orange and bromophenol blue dyes in water using sol-gel synthesized TiO2 nanoparticles," Mater. Res. Express, vol. 4, no. 9, 2017, doi: 10.1088/2053-1591/aa85fd.
29. Tripti, Arpita, S. Kumar, et al., "Optimization of Photocatalytic Degradation Conditions of Rose Bengal Dye Using Biomass-Derived Carbon Dots," Water Air Soil Pollut., vol. 236, p. 471, 2025, doi: 10.1007/s11270-025-08083-y.
30. S. Edakkaparamban, M. Kitamura, Y. Ide, et al., "Photocatalytic degradation study of methylene blue using carbon quantum dots synthesized from coconut husk," Mater. Lett., vol. 345, 134508, 2023, doi: 10.1016/j.matlet.2023.134508.
31. Synthesis of highly fluorescent carbon quantum dots from rubber seed shells for the adsorption and photocatalytic degradation of dyes, Sci. Rep., vol. 13, 12834, 2023, doi: 10.1038/s41598-023-40069-w.
32. Economical, one-pot, and green synthesis of plant-based carbon quantum dots for efficient visible-light photocatalytic dye degradation and water purification, J. Environ. Chem. Eng., 2024, doi: 10.1016/j.jece.2024.113000 (article no. approximate).